Ocean Dynamics (2016) 66:353–365
DOI 10.1007/s10236-016-0925-3

Ocean-atmosphere dynamics changes associated with prominent ocean surface turbulent heat fluxes trends during 1958–2013

Hu Yang[1] · Jiping Liu[2] · Gerrit Lohmann[1,3] · Xiaoxu Shi[1] · Yongyun Hu[4] · Xueen Chen[5]

Received: 3 May 2015 / Accepted: 11 January 2016 / Published online: 12 February 2016

Abstract Three prominent features of ocean surface turbulent heat fluxes (THF) trends during 1958–2013 are identified based on the Objectively Analyzed air-sea Fluxes (OAFlux) data set. The associated ocean-atmosphere dynamics changes are further investigated based on the National Centers for Environmental Prediction/National Center for Atmospheric Research (NCEP/NCAR) reanalysis. First, the THF are enhanced over the mid-latitude expansions of the subtropical western boundary currents (WBCs). An intensified oceanic heat transport, forced by stronger near-surface zonal wind, is likely to be the cause of such THF tendency. Second, the THF are reduced over the tropical eastern Pacific Ocean, which is primarily caused by the decreasing near-surface wind speed and sea surface temperature (SST), associated with a local coupled ocean-atmosphere cooling mode. Finally, the THF are reduced over the northern tropical Atlantic Ocean, which is attributed to the decreasing air-sea humidity and temperature differences as a result of the convergence of near-surface air and the divergence of ocean currents (upwelling).

Keywords Turbulent heat fluxes trend · Western boundary currents · Tropical eastern Pacific Ocean · Northern tropical Atlantic Ocean

Responsible Editor: Richard John Greatbatch

✉ Hu Yang
hu.yang0714@gmail.com

1 Alfred Wegener Institute, Helmholtz Centre for Polar and Marine Research, Bremerhaven, Germany

2 Department of Atmospheric and Environmental Sciences, University at Albany, State University of New York, New York NY, USA

3 Department of Environmental Physics, University of Bremen, Bremen, Germany

4 Department of Atmospheric and Oceanic Sciences, School of Physics, Peking University, Beijing, China

5 Physical Oceanography Laboratory, Ocean University of China, Qingdao, China

1 Introduction

Turbulent heat fluxes (THF) consist of two components: latent heat flux (LHF) and sensible heat flux (SHF). LHF is the flux of heat from the ocean to the atmosphere that is associated with evaporation. SHF is the conductive heat flux from the ocean to the atmosphere. As the main form of air-sea heat exchange, THF are of particular interest for the comprehensive understanding of the coupled ocean-atmosphere interactions.

Several studies have addressed the THF trends and their associated mechanisms in different regions and for varying periods. As reported by Tomita and Kubota (2005), the THF have increased during the 1990s over the Kuroshio-Oyashio extension region and reached their maximum during the past half century due to a pronounced warming in sea surface temperature (SST). By examining the variability of the LHF during 1989–2000, Liu and Curry (2006) found an increasing LHF associated with a positive trend of near-surface wind speed over the tropical and subtropical regions. Zhang et al. (2010a) showed that the LHF dampens the increase in SST caused by oceanic advection in the coastal China Seas during 1948–2006. Iwasaki and Kubota (2011) demonstrated that the LHF and freshwater flux were strengthened over the north-eastern subtropical

Pacific during 1988–2005. Based on the National Centers for Environmental Prediction/National Center for Atmospheric Research (NCEP/NCAR) reanalysis, Shaman et al. (2010) pointed out that THF have increased over the Gulf Stream during 1948–2008 mainly due to higher storm frequency. The extreme THF events over the subtropical western boundary currents (WBCs), as described by Gulev and Belyaev (2012), have increased significantly during the same period. By analyzing the Goddard Satellite-based Surface Turbulent Fluxes (GSSTF), Gao et al. (2013) also found an increase in the LHF over the Kuroshio Current and Gulf Stream during 1988–2008. On the basis of investigating the relationship between SST and THF on different time scales, Gulev et al. (2013) emphasized that on multi-decadal time scales, the ocean drives the atmosphere variability, whereas the opposite case is true for shorter timescales over the North Atlantic region (35–50° N). Given all above results, investigating the THF variability is of crucial importance for understanding and evaluating the climate feedbacks and changes.

This study aims to assess the long-term changes of the coupled ocean-atmosphere dynamics by examining the prominent sea surface THF trends. The International Comprehensive Ocean-Atmosphere Data Set (ICOADS) is the longest and most extensive collection of surface marine meteorological data mainly from ships and buoys since 1662 (Woodruff et al. 2011). However, the ICOADS suffers serious spatial/temporal sampling problems and measurement uncertainties (Da Silva et al. 1994; Chou et al. 2004; Gulev et al. 2007a). Regions with continuous ship observations are sparse. As in Gulev et al. (2013), they only evaluated the North Atlantic region, where a large number of ship observations are available over a long period of time. Recent satellite-based data products could overcome the shortcoming of spatial/temporal sampling problems, but are insufficient to study the long-term climate variability due to a lack of temporal coverage, as the data sets only cover relatively short period from 1987 to today. These products include the GSSTF v3 (Chou et al. 2003), the Hamburg Ocean Atmosphere Parameters and Fluxes from Satellite data (HOAPS) (Andersson et al. 2010), the Japanese Ocean Flux Data Sets with Use of Remote Sensing Observations (J-OFURO) (Kubota et al. 2002), and the Ocean Surface Turbulent Flux (SeaFlux) (Liu et al. 2011; Clayson and Bogdanoff 2013). The Objectively Analyzed air-sea Fluxes (OAFlux) are constructed from an optimal blending of surface meteorological variables from satellite retrievals and atmospheric reanalysis since 1958 (Yu and Weller 2007; Yu et al. 2008). Compared with ICOADS and satellite data sets, OAFlux fulfill the requirement of both acceptable accuracy and spatial/temporal coverage for this study.

The data sets used here, together with the method employed to identify the dominant factors for the THF trends, are introduced in the next section. In Section 3.1, the prominent THF trends and their dominant factors are examined. We try to explore the physical mechanisms behind the THF trends in Section 3.2. Finally, discussion and conclusions are presented in Sections 4 and 5, respectively.

2 Data and method

2.1 Data

The OAFlux use the objective analysis to obtain optimal estimates of flux-related surface meteorology and then computes the global fluxes by applying the state-of-the-art COARE bulk flux algorithm 3.0 (Fairall et al. 2003). The surface meteorological fields used in OAFlux are derived from satellite remote sensing and reanalysis outputs. OAFlux have several versions of THF products with different spatial and temporal resolutions, i.e., monthly 1-degree resolution (1958 onward), daily 1-degree resolution (1985 onward), and daily 0.25-degree resolution (1987 onward). Different input data sources are blended in different versions of OAFlux. In this work, the monthly 1-degree resolution of OAFlux, spanning 1958–2013, is used to study the prominent THF trends. This version of OAFlux blends three atmosphere reanalysis (i.e., NCEP/NCAR, NCEP/DOE and ERA-40) and four satellite products (i.e., OISST, SSM/I, AMSR-E, and QuikSCAT). Furthermore, it has been validated against in situ flux measurements. Note that, before 1985, only atmosphere reanalysis data sets are blended in this version. After 1985, both satellite data and atmosphere reanalysis are synthesized (Yu and Weller 2007; Yu et al. 2008).

Another set of data used in this work is the NCEP/NCAR reanalysis, which is a long-term data set based on a frozen global data assimilation and observational data from a variety of sources, i.e., weather stations, ships, buoys, aircrafts, radiosondes, and satellites (Kalnay et al. 1996). The NCEP/NCAR spans from 1948 to 2013 with a spatial resolution of T62 (approximately 210 km at the equator).

The monthly mean THF (positive-upward) along with flux-related input state parameters from the OAFlux data set, and the monthly mean atmosphere parameters (i.e., near-surface wind, sea level pressure, SST, surface air temperature, surface specific humidity) from the NCEP/NCAR data set are used in our study. The OAFlux are used to investigate the prominent THF trends, and the NCEP/NCAR is utilized to interpret the associated ocean-atmosphere dynamic changes. Besides, NCEP/NCAR data set also serves as a cross validation of the THF trends from the perspective of climate dynamics.

2.2 Method

The THF depend primarily on near-surface wind speed, air-sea humidity, and temperature differences, as described in the COARE bulk flux algorithm 3.0 (Fairall et al. 2003):

$$\mathrm{LHF} = \rho_a L C_E U_a (q_s - q_a) \tag{1}$$

$$\mathrm{SHF} = \rho_a c_p C_H U_a (T_s - T_a) \tag{2}$$

where ρ_a is the surface air density, L is the latent heat of vaporization for water, c_p is the specific heat of air at constant pressure, C_E and C_H represent the bulk transfer coefficients for humidity and temperature, respectively. U_a stands for the near-surface wind speed. q_s and q_a are the surface saturation humidity and surface specific humidity, T_s and T_a are the SST and surface air temperature, respectively. Taking into account the effect of salinity, q_s is usually computed as $0.98 q_{sat}(T_s)$, where q_{sat} represents the saturation humidity for pure water at T_s. In addition, T_a includes a correction from the measured surface air temperature T_z at the height z, using the adiabatic lapse rate γ, as $T_a = T_z + \gamma z$.

In order to identify the dominant factors that are responsible for the THF variability, we divide U_a, q_s, q_a, T_s, and T_a into the climatological means and the anomaly terms ($U_a = \overline{U_a} + U_a'$, $q_s = \overline{q_s} + q_s'$, $q_a = \overline{q_a} + q_a'$, $T_s = \overline{T_s} + T_s'$, $T_a = \overline{T_a} + T_a'$). The overbar denotes the climatological mean and the prime denotes anomaly. Since the anomaly terms of each variable are much smaller than the climatological means (mostly less than 10 %), Eqs. 1 and 2 can be linearized by the same method as in (Tanimoto et al. 2003):

$$\mathrm{LHF}' \approx \rho_a L C_E (L_{q_s} + L_{q_a} + L_{U_a}) \tag{3}$$

$$\mathrm{SHF}' \approx \rho_a c_p C_H (S_{T_s} + S_{T_a} + S_{U_a}) \tag{4}$$

Here, LHF′ and SHF′ represent the anomalies of LHF and SHF, L_{q_s}, L_{q_a}, L_{U_a}, S_{T_s}, S_{T_a}, and S_{U_a} refer to $\overline{U_a} q_s'$, $-\overline{U_a} q_a'$, $(\overline{q_s} - \overline{q_a}) U_a'$, $\overline{U_a} T_s'$, $-\overline{U_a} T_a'$, $(\overline{T_s} - \overline{T_a}) U_a'$, in Eqs. 6 and 7 in Tanimoto et al. (2003), respectively. L_{q_s}, L_{q_a}, and L_{U_a} can be treated as the respective contributions from q_s', q_a', and U_a' to the total LHF anomaly. S_{T_s}, S_{T_a} and S_{U_a} represent the respective contributions from the T_s', T_a' and U_a' to the total SHF anomaly.

Finally, we introduce two indices CL_X and CS_X to quantify the relative importance of the terms in Eqs. 3 and 4 :

$$CL_X = \frac{|L_X|}{|L_{q_s}| + |L_{q_a}| + |L_U|} \tag{5}$$

$$CS_X = \frac{|S_X|}{|S_{T_s}| + |S_{T_a}| + |S_U|} \tag{6}$$

For Eq. 5, CL_X represents the relative importance of either the surface saturation humidity (in this case $X = q_s$), surface specific humidity (i.e., $X = q_a$)) or the near-surface wind speed (i.e., $X = U_a$). The denominator of the right side ($|L_{q_s}| + |L_{q_a}| + |L_U|$) stands for the total contribution of the three influencing factors to the LHF anomaly. By such definition, CL_X ranges from 0 to 1, and a larger CL_X indicates a more dominated contribution by the variable X to the LHF anomaly. If CL_X exceeds 0.5, the term X basically dominates the LHF anomaly. Therefore, we define the X with $CL_X > 0.5$ as the dominant factor causing the LHF anomaly. A similar definition applies to the SHF in Eq. 6 as well, and X in Eq. 6 represents the SST (T_s), surface air temperature (T_a), or the near-surface wind speed (U_a).

To interpret the long-term trends, all our analysis is based on annual mean values. However, we note that both the THF and the flux-related parameters have a seasonal variability. Finally, as the linearization of the bulk flux formulae no longer applies over high latitude (Liu et al. 1979; Bourassa et al. 2013), we only present the results between 50° S–50° N in this work.

3 Results

3.1 Identification of prominent THF trends and associated dominant factors

The linear trends of THF from OAFlux, as depicted in Fig. 1a, exhibit three prominent features: (1) a significant increase in the THF occurs over the mid-latitude expansions of the primary subtropical WBCs (i.e., the Kuroshio Current, the Gulf Stream, the Agulhas Current, the Eastern Australian Current, and the Brazil Current) with a magnitude of ∼8–12 W/m^2 per decade; (2) a pronounced decrease in the THF happens over the tropical eastern Pacific Ocean at the rate of ∼6–10 W/m^2 per decade; and (3) over the northern tropical Atlantic Ocean the THF reduce at a speed of ∼4–6 W/m^2 per decade. These three prominent features of THF′ are also observed in the LHF and SHF trends (Fig. 1b, c), with almost equivalent magnitudes for the former and, however, a less pronounced pattern for the latter, indicating an overwhelming contribution of LHF′ to the THF trends.

To identify the dominant factors which are responsible for the prominent THF trends, we compute the trends of the q_s, q_a, T_s, T_a, and U_a, respectively (Figs. 2 and 3). The CL_X and CS_X are further calculated based on the climatology mean and linear trends of each parameter (see Eqs. 5 and 6).

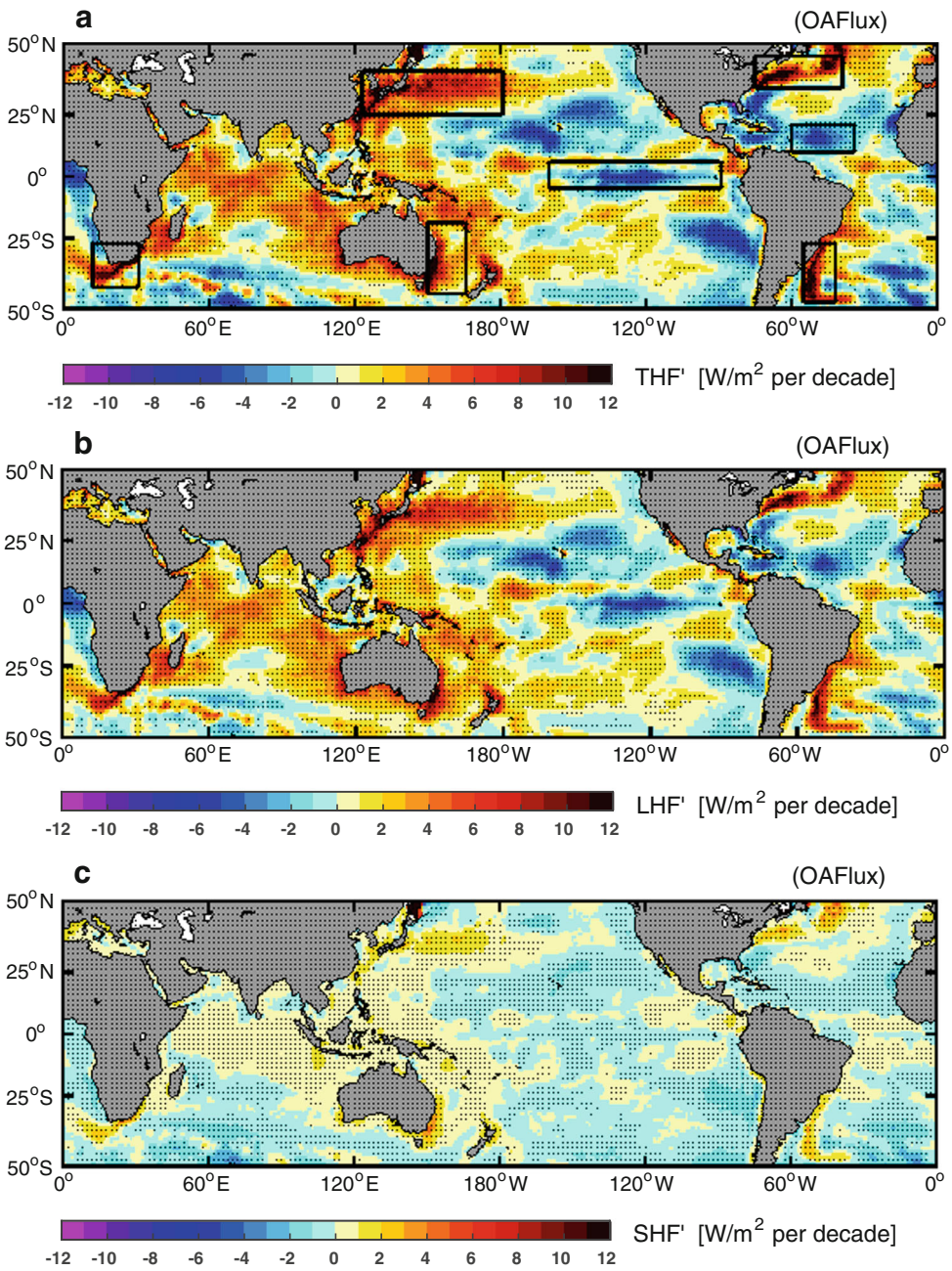

Fig. 1 Spatial distributions of trends in turbulent heat fluxes (THF′, **a**), latent heat flux (LHF′, **b**) and sensible heat flux (SHF', **c**) in OAFlux data set. Stippling indicates regions where the trends pass the 90 % confidence level (Student's t test). The *black rectangles* locate the regions where we interpret the THF trends

The areas with $CL_X > 0.5$ and $CS_X > 0.5$ are marked with black crosses in Figs. 2 and 3.

The paths of the primary WBCs experienced a significant increase in SST (Figs. 2a and 3a), which constitutes the dominating cause of LHF′ and SHF′ over the same regions. Meanwhile, the surface winds over these regions have accelerated, contributing to enhancing the ocean heat loss over there. Over the tropical eastern Pacific Ocean, we observe a significant decrease in SST (q_s and T_s) and U_a, both of which together contribute to the decreasing LHF and SHF over the tropical eastern Pacific Ocean. Furthermore, the reduced LHF and SHF over the northern tropical Atlantic Ocean is primarily associated with an increases in surface specific humidity (q_a) and surface air temperature (T_a) (Figs. 2b and 3b).

Having described the patterns of THF trends and their contributors, we turn to examine the time evolution of these factors. Since the surface specific humidity (q_a) is physically linked to the surface saturation humidity (q_s), their contributions to the LHF anomaly are treated together as a

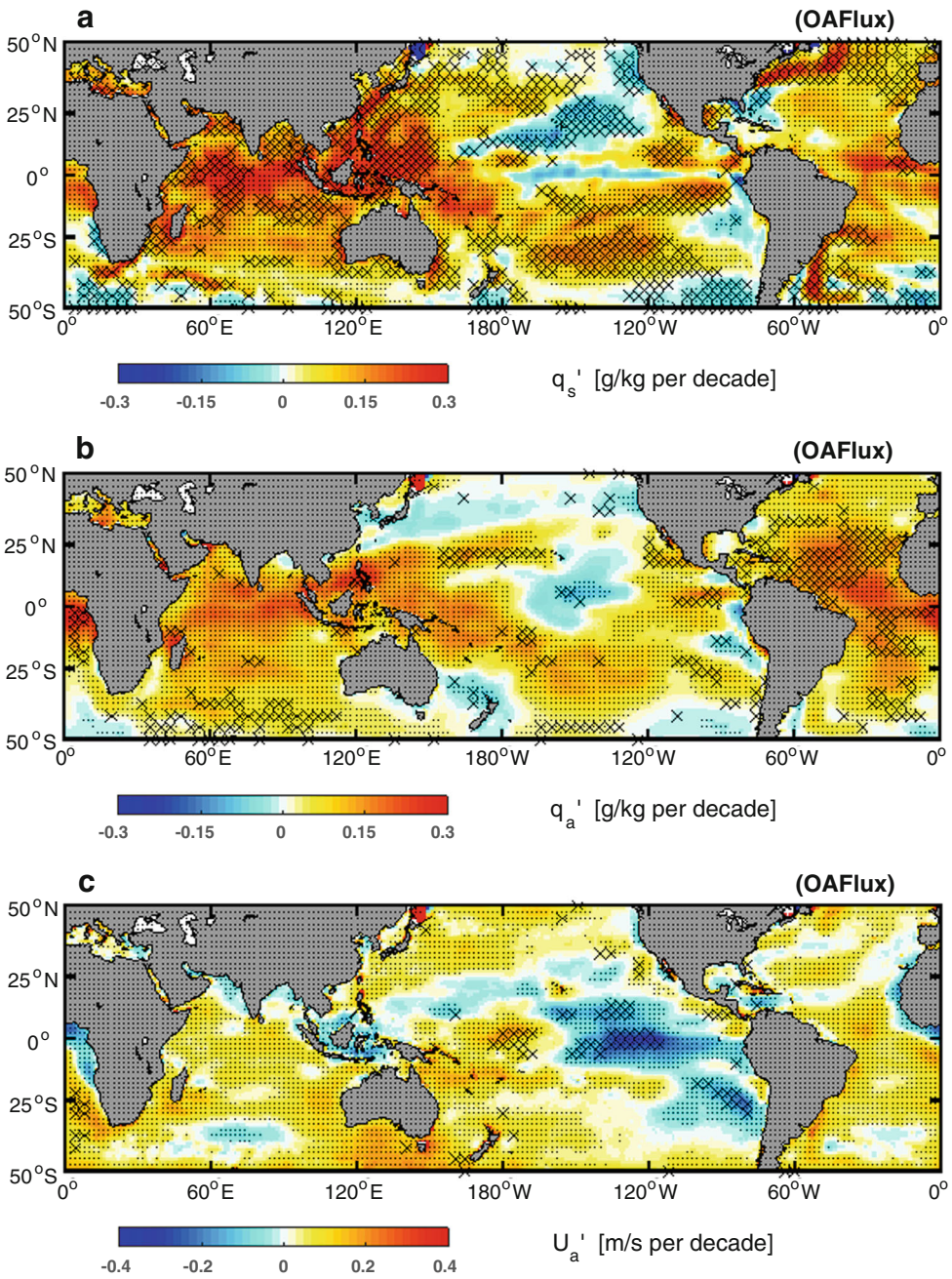

Fig. 2 As Fig. 1, spatial distributions of the trends in surface saturation humidity ($q_s{}'$, **a**), specific humidity ($q_a{}'$, **b**), and wind speed ($U_a{}'$, **c**). The area with $CL_X > 0.5$ (see Eq. 5) are marked with *black cross*

contribution by air-sea humidity difference ($L_{q_s} + L_{q_a}$). A similar assumption applies to the air-sea temperature difference (as $S_{T_s} + S_{T_a}$) in Fig. 4. We find that the increases in LHF and SHF over the WBCs mainly occur during 1970–2000. The air-sea humidity and temperature differences are the main drivers for the increases. For the tropical eastern Pacific Ocean, strong interannual variations of LHF and SHF are observed, which resemble the signal of the El Nino-Southern Oscillation (ENSO). While, on long time scales, the weakening surface wind plays an equivalent role as the reduced air-sea humidity and temperature differences in the decreasing THF. Regarding the northern tropical Atlantic, a continuous decline of air-sea humidity difference depresses the ocean THF loss there.

3.2 Possible mechanisms for the THF trends

3.2.1 Increasing THF over the WBCs

WBCs transport a large amount of heat from the low latitudes to the mid and high latitudes, which contribute to the Earth's energy balance. The heat release from the WBCs is primarily in the form of THF. Figure 3a describes the spatial distribution of SST trends during 1958–2013. It appears that

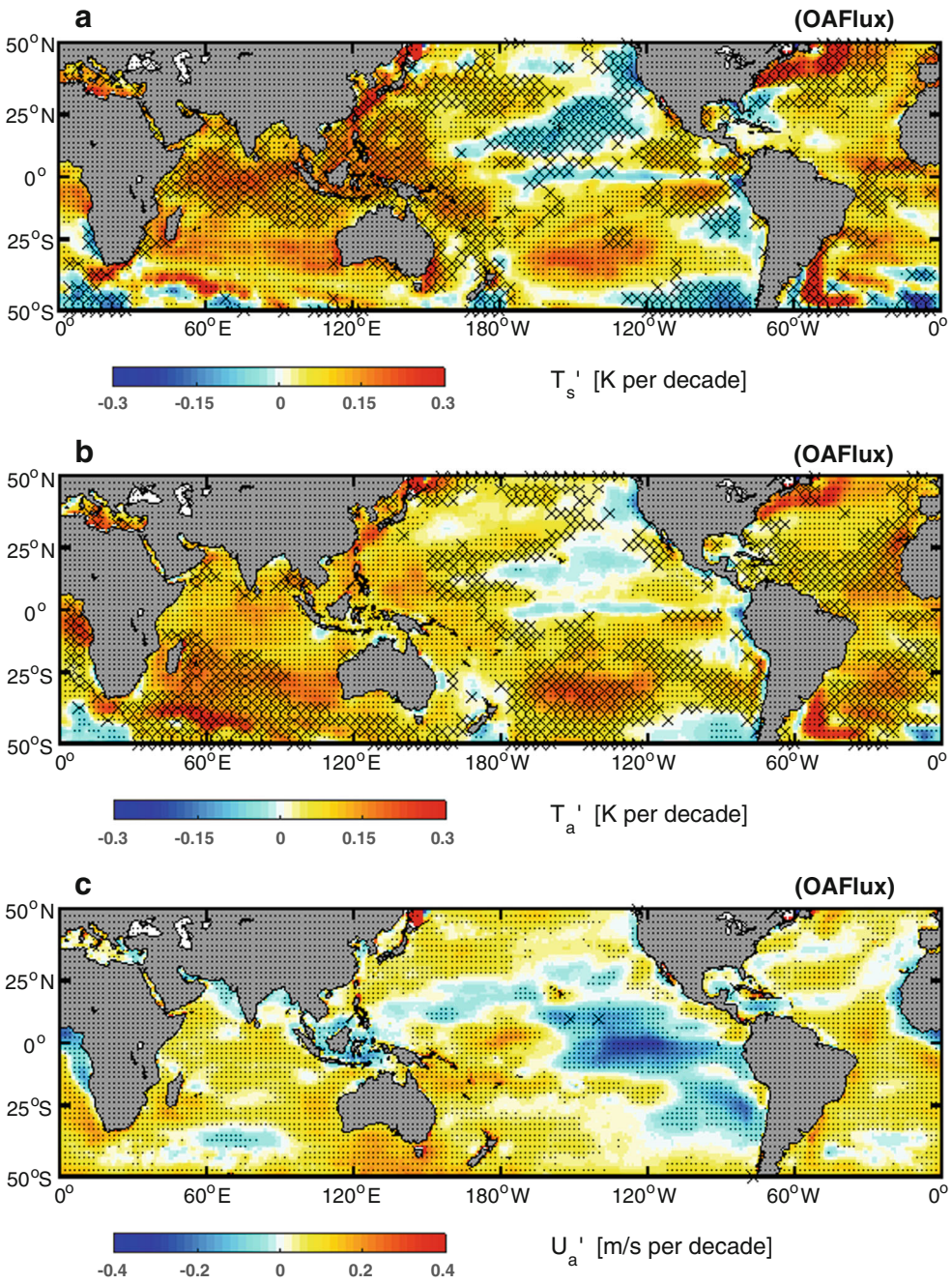

Fig. 3 As Fig. 1, spatial distributions of the trends in sea surface temperature (T_s', **a**), surface air temperature (T_a', **b**), and wind speed (U_a', **c**). The area with $CS_X > 0.5$ (see Eq. 6) are marked with *black cross*

there is an enhanced warming of the main WBCs, on a magnitude of ∼0.2–0.3 K per decade consistent with Wu et al. (2012). This is remarkably stronger than the SST increase at the same latitudes during the same period. As demonstrated in Section 3.1, the enhanced SST warming greatly strengthens the THF loss over the WBCs, indicating an ocean controlled climate trend. The THF in turn has a damping effect on the SST (Cayan 1992; Zhang and Mcphaden 1995; Frankignoul and Kestenare 2002). Moreover, from the perspective of ocean and atmosphere heat balance, increasing SST associated with enhanced THF loss implies that the heat transport by the WBCs has strengthened.

Figure 5 presents the trend and climatology of near-surface zonal wind stress. On one hand, the westerly winds over the mid and high latitudes are stronger in intensity. On the other hand, over most of the tropical regions, the easterly winds are also accelerated, except for the tropical eastern Pacific Ocean. The pattern correlation coefficient between the trend and climatology zonal wind is 0.54, with a 95 % confidence level (Student's t test), illustrating that

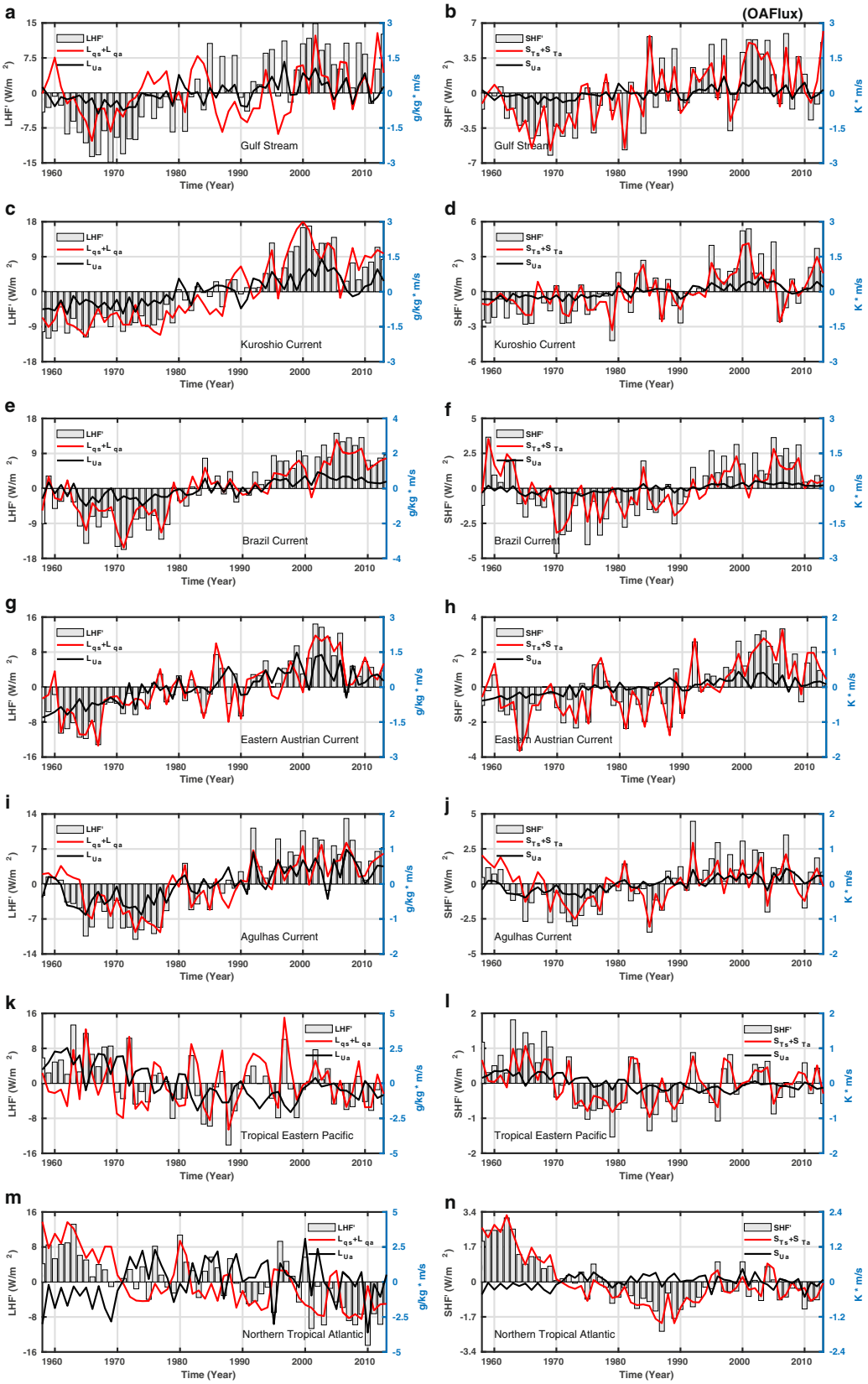

Fig. 4 Time series of area-averaged LHF (**a, c, e, g, i, k, m**) and SHF (**b, d, f, h, j, l, n**) anomalies (*grey bar*) and their corresponding contributors (*red and black lines*) over the identified regions (as shown in Fig. 1a). The left axis is for the heat flux anomaly (i.e. LHF′, SHF′), and the right axis is for the THFs contribution terms (i.e., L_{q_s}, L_{q_a}, L_{U_a}, S_{T_s}, S_{T_a}, S_{U_a})

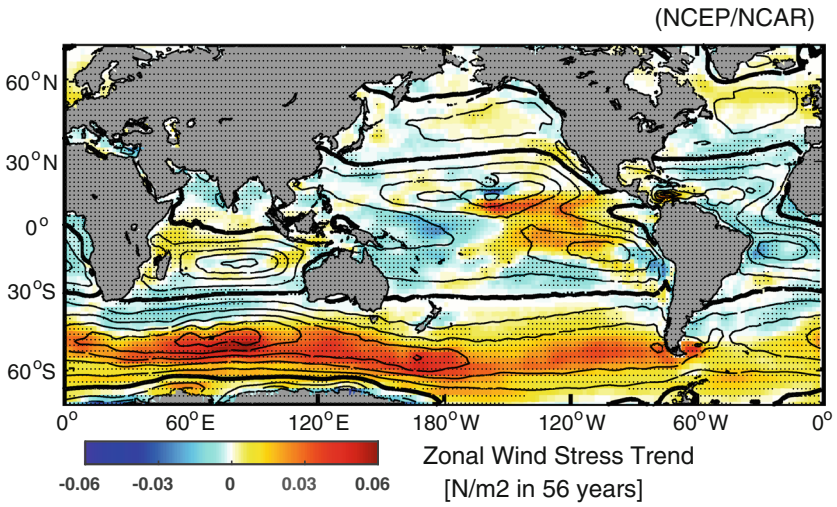

Fig. 5 Spatial distributions of the trend (shading, westerly-positive) and climatology (contours) of zonal wind stress. Easterly wind stress is in *dash lines*, westerly wind stress is in *solid lines*, and zero zonal wind stress is *bold*

the background surface wind circulation has strengthened in the latitude belts approximately between 10° and 65° in both hemispheres. Note that the stronger westerly winds are more pronounced over the Southern Hemisphere than that over the Northern Hemisphere.

According to the Sverdrup's theory of oceanic circulation, wind stress curl between the low latitudes and mid-latitudes is the main driver of the subtropical gyres. We compute the averaged wind stress curl over the corresponding subtropical gyres (as shown in Fig. 6a). It comes out

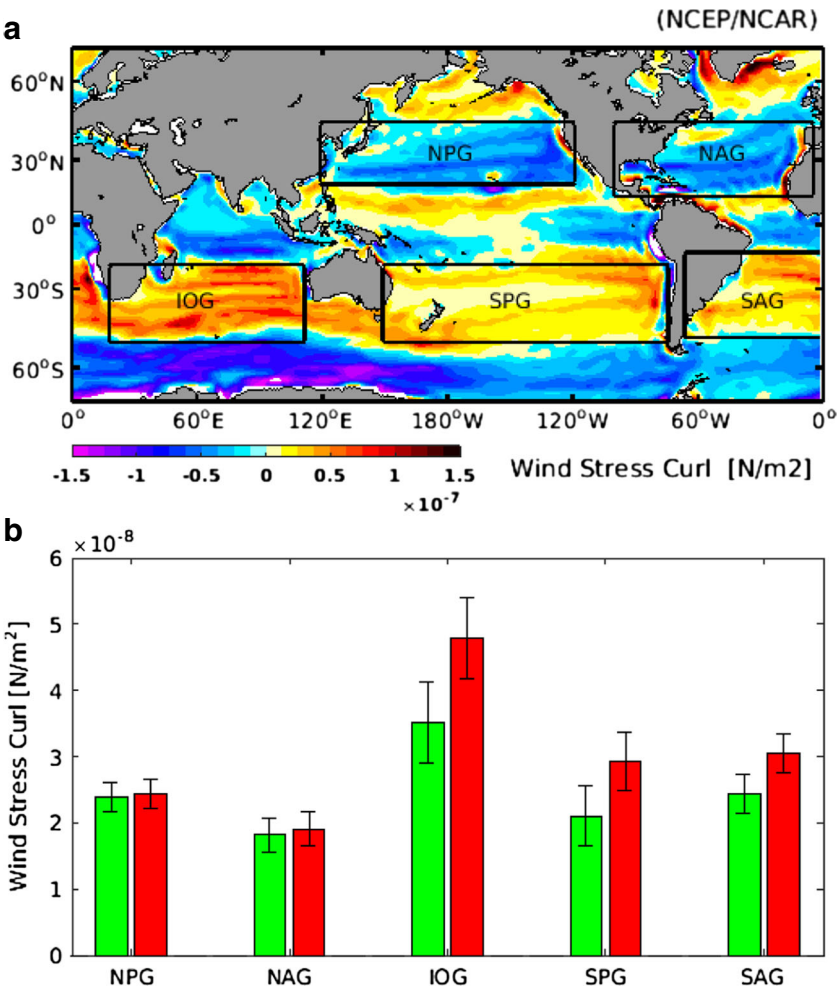

Fig. 6 **a** Spatial distribution of the climatological ocean surface wind stress curl. The *black rectangles* locate the area where we compute the area-mean wind stress curl. **b**. Absolute values of area-mean wind stress curl over the corresponding subtropical gyres shown in the *upper panel*. *Red* and *green bars* denote mean ± trend/2, with *error bars* indicating their corresponding standard deviations. *NPG* North Pacific Gyre, *NAG* North Atlantic Gyre, *IOG* India Ocean Gyre, *SPG* South Pacific Gyre, *SAG* South Atlantic Gyre

that the magnitude of wind stress curl has increased over all the five subtropical gyres (Fig. 6b). The intensification of both the low latitude easterly and mid-latitude westerly (Fig. 5) would strengthen the subtropical wind stress curl, which forces stronger WBCs. Even though the intensification of zonal wind stress (or subtropical wind stress curl) over the Northern Hemisphere is not significant, it could have an amplifying effect over the WBCs through the ocean dynamic feedback. The WBCs in turn transport more heat and accelerate the THF loss over the mid-latitude expansions of these currents. It is worth noting that further analyses based on the European Centre for Medium-Range Weather Forecasts 40-year Reanalysis (ERA40, covering 1958–2001) (Uppala et al. 2005) reveal similar patterns as the NCEP/NCAR (not shown), indicating that the results found here are not dataset-dependent.

3.2.2 Decreasing THF over the tropical eastern Pacific Ocean

The decreased SST over the eastern tropical Pacific Ocean, as depicted in Fig. 7a, shows good agreement with the OAFlux (Fig. 3a). Such cooling limits the heat loss from ocean surface. Meanwhile, the cooling SST is coupled with a sinking air flow, accompanied by a positive SLP trend (shading in Fig. 7b) and a divergence tendency of near-surface winds (vectors in Fig. 7a, b). The divergence of near-surface winds over the eastern Pacific weakens the background easterly trade winds and reduces the wind speed there. The combined effects of both the decreased SST and the weakened wind speed suppress the ocean surface THF loss.

3.2.3 Decreasing THF over the northern tropical Atlantic Ocean

To investigate the negative THF trend over the northern tropical Atlantic Ocean, we present the trends of near-surface wind, and air-sea humidity and temperature differences in Fig. 8. During 1958–2013, there is a strengthening of easterly winds over the northern subtropical Atlantic and south-easterly winds near the equatorial Atlantic. Such wind anomalies tend to induce an Ekman divergence of the ocean current (upwelling) over the northern tropical Atlantic Ocean, which cools the ocean surface. By contrast, such

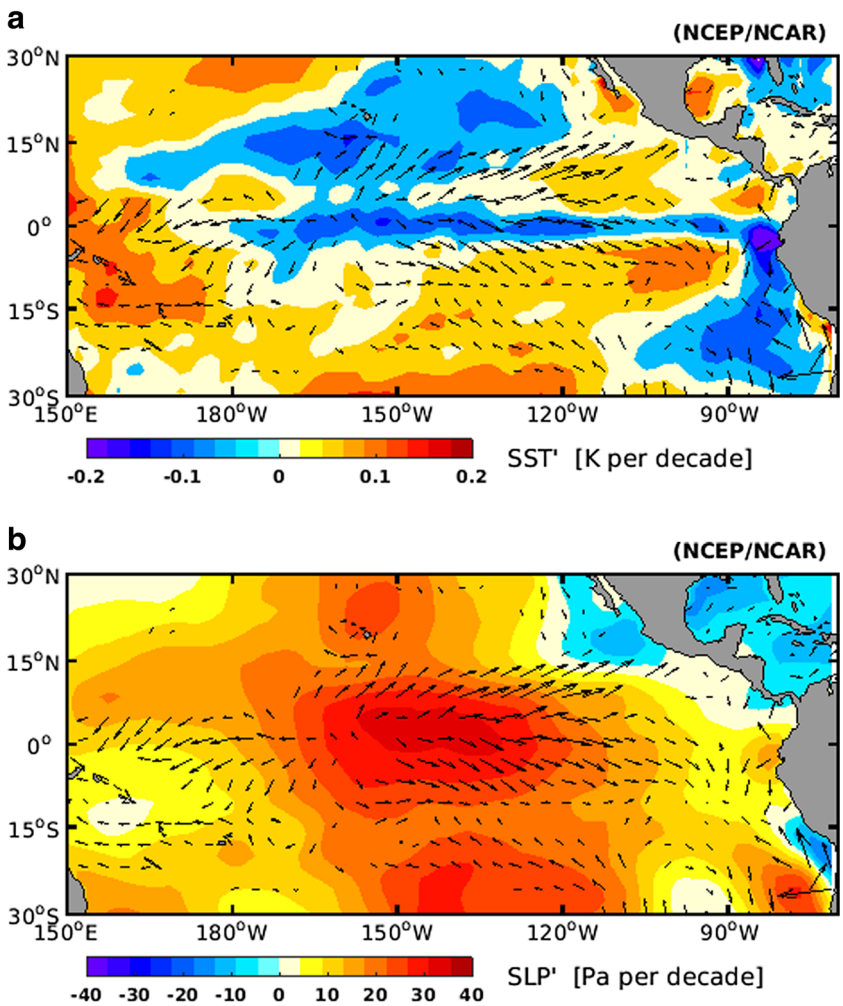

Fig. 7 Trends in surface wind (vectors), SST (**a**, shading) and SLP (**b**, shading) over the Pacific Ocean. We only show the wind trend above 90 % confidence level (Student's *t* test)

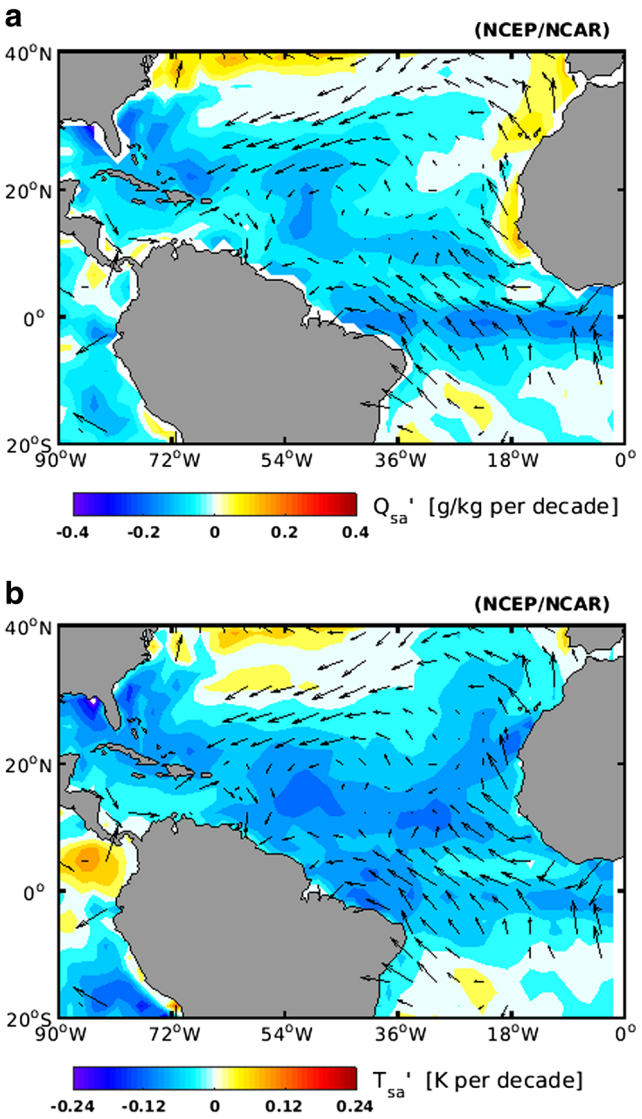

Fig. 8 Trends in surface wind (vectors), air-sea humidity difference (**a**, shading) and air-sea temperature difference (**b**, shading) over the Atlantic Ocean

pattern of wind trend results in a convergence of near-surface air at the same region, which provides a source of heat and water vapor from the adjacent area, contributing to the increases in the q_a (Fig. 2b) and T_a (Fig. 3b) there. Therefore, both the strengthening of easterly winds over the northern subtropical Atlantic and the intensified south-easterly winds near the equatorial Atlantic constitute the cause of the reduced air-sea humidity and temperature differences, which together suppress the ocean heat loss there.

4 Discussion

Due to the differences in the source of input variables, the formulation of bulk algorithms, and the changes in the observing system, uncertainties still remain in the THF data sets (Kalnay et al. 1996; Zeng et al. 1998; Moore and Renfrew 2002; Curry et al. 2004; Yu et al. 2008; Santorelli et al. 2011; Brunke et al. 2011). Considering the existing uncertainties in the heat flux data sets, we only focus on the prominent THF trends in this work. The THF trends we have identified are consistent with other studies. For example, Yu et al. (2008) showed that the increased LHF over the WBCs primarily occurs after the 1970s. Based on GSSTF data set, Gao et al. (2013) reported that the maximum LHF increases occur over the WBCs regions during 1988–2008. Additionally, their pattern of LHF trends also suggests that the LHF increases over the tropical Eastern Pacific and northern tropical Atlantic Ocean are relatively small compared to the overwhelming increase LHF over the tropical ocean surface (see Gao et al. (2013), Fig. 2).

In this study, we interpolate the THF trends based on annual mean values. However, THF have seasonal variations, particularly over the mid and high latitudes. In different seasons, the THF trends may vary depending on the flux-related state variables and different physical mechanism (Gulev et al. 2007b; Gulev and Belyaev 2012). Yu et al. (2008) pointed out that the THF over the WBCs increased mainly during wintertime, associated with increasing storm frequency (Shaman et al. 2010; Gulev and Belyaev 2012). In our analysis, we also find that the near-surface wind speed over the WBCs has accelerated, which is likely linked to higher storm activities. In the future, a comprehensive study on the seasonal THF trends and their contributors are essential to further understand the mechanism and the climate consequence.

Due to natural variability, trend estimates are sensitive to the analyzed time periods, especially when the period is short. To assess the long-term changes of the coupled ocean atmosphere dynamics, we choose a relatively long period (56 years, 1958–2013) to carry out this work. However, the presented trends could also reflect climate variations on multi-decadal time scales. For example, the THF over the Kuroshio Current and the Gulf Stream increase primarily during 1970–2000 (as in Fig. 4). The variations seem to be associated with an increase of the Arctic Oscillation starting from the late 1960s to the 1990s, which manifests in stronger westerly winds over the North Hemisphere (Thompson and Wallace 2000). But the Arctic Oscillation shifted towards a negative phase after the 1990s. Over the Southern Hemisphere, an increase of the Antarctic Oscillation is also observed, which explains the strengthening Southern Hemisphere westerly (Thompson and Wallace 2000; Marshall 2003). However, we notice that the THF over the Brazil Current and the Agulhas Current also show strong decadal variations (see Fig. 4), which contribute to the increase THF at this certain period. To conclude whether the identified THF trends reflect long-term climate trends

or multi-decadal variations, observations with a longer time interval are required.

The WBCs play a vital role in the climate over the adjacent mainland (Minobe et al. 2008; Kelly et al. 2010). Previously, the strengthening WBCs has been documented individually, for example, the Gulf Stream (Curry and McCartney 2001), the Kuroshio Current (Qiu and Joyce 1992; Deser et al. 1999; Sato et al. 2006; Sakamoto et al. 2005), and the Eastern Australia Current (Cai et al. 2005; Qiu and Chen 2006; Ridgway 2007; Roemmich et al. 2007; Ridgway et al. 2008). Curry and McCartney (2001) found that transport of the Gulf Stream has intensified after the 1960s. Sato et al. (2006) and Sakamoto et al. (2005) projected a stronger Kuroshio Current in response to global warming according to a high-resolution coupled atmosphere-ocean climate model. Based on long-term temperature and salinity observations from an ocean station off eastern Tasmania, Ridgway (2007) demonstrated that the East Australian Current had increased over the past 60 years. Beyond these studies on individual WBCs, our study suggests that the climate change over the WBCs is likely to be a systematic phenomenon over all ocean basins. As Wu et al. (2012) also stressed, there was enhanced SST warming over all the WBCs. However, controversy still remains on the dynamic changes of WBCs due to the uncertainty of the data sets. According to a continuous observation from undersea telephone cables near 27° N in the Straits of Florida, DiNezio et al. (2009) constructed a time series of transport of the Florida Current (part of Gulf Stream) since 1982. The time series suggest no indication of positive trend during the covering period (1982–2007).

Considering the tropical eastern Pacific, Cane et al. (1997) and Zhang et al. (2010b) observed a cooling mode of the Pacific cold tongue under global warming associated with an increased upwelling (Cane et al. 1997). Model experiments show that the cooling over the tropical eastern Pacific leads the ocean to absorb more heat from the atmosphere, contributing to the global warming hiatus in recent decades (Meehl et al. 2011; Kosaka and Xie 2013). However, the cooling mode is very likely to collapse in the future, as suggested by the coupled climate models (Meehl et al. 2011). Regarding the northern tropical Atlantic Ocean, the trend of wind speed is very likely to be a stronger regime of the Intertropical Convergence Zone (ITCZ) which is characterized by a convergence of surface air and divergence of ocean currents.

The THF are related to the energy and water vapor transport from the ocean to the atmosphere. Prominent THF trends can be an indicator for the remarkable changes in the ocean and atmosphere dynamics. Besides the three identified THF trends in this paper, there are some other regions where the THF trends are significant, i.e., the decreased THF over the northern subtropical central Pacific, the reduced THF over the southern subtropical eastern Pacific. These trends are also worth being investigated in the future. In addition, the seasonal dependence of THF trends and their corresponding impact factors are beyond the scope of this paper, which are of particular importance for understanding the mechanisms.

5 Conclusions

Based on the OAFlux data set, we have recognized three prominent ocean surface THF trends during 1958–2013, i.e., the enhanced THF over the mid-latitude expansions of subtropical WBCs, the reduced THF over the tropical eastern Pacific Ocean, and the reduced THF over the northern tropical Atlantic Ocean.

The dominant factors for these THF trends are identified by linearizing the bulk flux formulae. We find that over the WBCs, the THF are enhanced by the increasing SST. Such change is likely to be induced by intensified WBCs which are forced by a systemic stronger near-surface zonal wind stress in the latitude belts approximately between 10° and 65° in both hemispheres. Over the tropical eastern Pacific Ocean, the THF are reduced primarily through the decreasing near-surface wind speed and SST. The associated dynamic changes are found to be the divergence of near-surface wind coupled with a cooling ocean surface over the tropical Pacific Ocean. Over the northern tropical Atlantic Ocean, the reduced THF are primarily affected by the increasing surface specific humidity and air temperature, corresponding with a convergence of surface air and divergence of ocean currents.

This work proposes a novel way of exploring the changes of atmosphere-ocean dynamics by examining the trends of THF. As a next step, the associated dynamic changes will be investigated with more data sets and model scenarios.

Acknowledgments We would like to thank Wei Wei, Mihai Dima, and Xun Gong for their helpful discussions, and Stefanie Klebe for her friendly review. Jiping Liu is supported by the NOAA Climate Observations and Monitoring Program (NA14OAR4310216) and NASA NEWS. The co-author Chen Xueen's position is also supported by Taishan scholars program.

References

Andersson A, Fennig K, Klepp C, Bakan S, Graßl H, Schulz J (2010) The Hamburg Ocean Atmosphere Parameters and Fluxes from Satellite Data-HOAPS-3. Earth System Science Data Discussions 3:143–194

Bourassa MA, Gille ST, Bitz C, Carlson D, Cerovecki I, Clayson CA, Cronin MF, Drennan WM, Fairall CW, Hoffman RN et al (2013) High-latitude ocean and sea ice surface fluxes: challenges for climate research. Bull Am Meteorol Soc 94(3):403–423

Brunke MA, Wang Z, Zeng X, Bosilovich M, Shie CL (2011) An assessment of the uncertainties in ocean surface turbulent fluxes in 11 reanalysis, satellite-derived, and combined global datasets. J Clim 24(21):5469–5493

Cai W, Shi G, Cowan T, Bi D, Ribbe J (2005) The response of the Southern Annular Mode, the East Australian Current, and the southern mid-latitude ocean circulation to global warming. Geophys Res Lett 32(23):L23,706

Cane M, Clement A, Kaplan A, Kushnir Y, Pozdnyakov D, Seager R, Zebiak S, Murtugudde R (1997) Twentieth-century sea surface temperature trends. Science 275(5302):957–960

Cayan DR (1992) Latent and sensible heat flux anomalies over the northern oceans: driving the sea surface temperature. J Phys Oceanogr 22(8):859–881

Chou SH, Nelkin E, Ardizzone J, Atlas RM, Shie CL (2003) Surface turbulent heat and momentum fluxes over global oceans based on the Goddard satellite retrievals, version 2 (GSSTF2). J Clim 16(20):3256–3273

Chou SH, Nelkin E, Ardizzone J, Atlas RM (2004) A comparison of latent heat fluxes over global oceans for four flux products. J Clim 17(20):3973–3989

Clayson CA, Bogdanoff AS (2013) The effect of diurnal sea surface temperature warming on climatological air–sea fluxes. J Clim 26(8):2546–2556

Curry J, Bentamy A, Bourassa M, Bourras D, Bradley EF, Brunke M, Castro S, Chou S, Clayson C, Emery W et al (2004) Seaflux. Bull Am Meteorol Soc 85(3):409–424

Curry RG, McCartney MS (2001) Ocean gyre circulation changes associated with the North Atlantic Oscillation. J Phys Oceanogr 31(12):3374–3400

Da Silva A, Young C, Levitus S (1994) Atlas of surface marine data 1994, vol. 1, Algorithms and Procedures, NOAA Atlas NESDIS 6. US Dep of Commer, Washington, DC

Deser C, Alexander M, Timlin M (1999) Evidence for a wind-driven intensification of the Kuroshio Current Extension from the 1970s to the 1980s. J Clim 12(6):1697–1706

DiNezio PN, Gramer LJ, Johns WE, Meinen CS, Baringer MO (2009) Observed interannual variability of the Florida Current: Wind forcing and the North Atlantic Oscillation. J Phys Oceanogr 39(3):721–736

Fairall C, Bradley EF, Hare J, Grachev A, Edson J (2003) Bulk parameterization of air-sea fluxes: updates and verification for the COARE algorithm. J Clim 16(4):571–591

Frankignoul C, Kestenare E (2002) The surface heat flux feedback. Part I: estimates from observations in the Atlantic and the North Pacific. Clim Dyn 19(8):633–647. doi:10.1007/s00382-002-0252-x

Gao S, Chiu LS, Shie CL (2013) Trends and variations of ocean surface latent heat flux: Results from GSSTF2c data set. Geophysical Research Letters

Gulev S, Jung T, Ruprecht E (2007a) Estimation of the impact of sampling errors in the VOS observations on air-sea fluxes. Part I: uncertainties in climate means. J Clim 20(2):279–301

Gulev S, Jung T, Ruprecht E (2007b) Estimation of the impact of sampling errors in the VOS observations on air-sea fluxes. Part II: impact on trends and interannual variability. J Clim 20(2):302–315

Gulev SK, Belyaev K (2012) Probability distribution characteristics for surface air-sea turbulent heat fluxes over the global ocean. J Clim 25(1):184–206

Gulev SK, Latif M, Keenlyside N, Park W, Koltermann KP (2013) North Atlantic Ocean control on surface heat flux on multidecadal timescales. Nature 499:464–467

Iwasaki S, Kubota M (2011) Increasing trends for the surface heat flux and fresh water flux in the North Pacific eastern subtropical region. Geophys Res Lett 38(10):L10,604

Kalnay E, Kanamitsu M, Kistler R, Collins W, Deaven D, Gandin L, Iredell M, Saha S, White G, Woollen J et al (1996) The NCEP/NCAR 40-year reanalysis project. Bull Am Meteorol Soc 77(3):437–471

Kelly KA, Small RJ, Samelson R, Qiu B, Joyce TM, Kwon YO, Cronin MF (2010) Western boundary currents and frontal air-sea interaction: Gulf Stream and Kuroshio Extension. J Clim 23(21):5644–5667. doi:10.1175/2010JCLI3346.1

Kosaka Y, Xie SP (2013) Recent global-warming hiatus tied to equatorial Pacific surface cooling. Nature 501(7467):403–407

Kubota M, Iwasaka N, Kizu S, Konda M, Kutsuwada K (2002) Japanese ocean flux data sets with use of remote sensing observations (J-OFURO). J Oceanogr 58(1):213–225

Liu J, Curry J (2006) Variability of the tropical and subtropical ocean surface latent heat flux during 1989–2000. Geophys Res Lett 33:L05,706

Liu J, Curry JA, Clayson CA, Bourassa MA (2011) High-resolution satellite surface latent heat fluxes in North Atlantic hurricanes. Mon Weather Rev 139(9):2735–2747

Liu WT, Katsaros KB, Businger JA (1979) Bulk parameterization of air-sea exchanges of heat and water vapor including the molecular constraints at the interface. J Atmos Sci 36(9):1722–1735

Marshall GJ (2003) Trends in the Southern Annular Mode from observations and reanalyses. J Clim 16(24):4134–4143

Meehl GA, Arblaster JM, Fasullo JT, Hu A, Trenberth KE (2011) Model-based evidence of deep-ocean heat uptake during surface-temperature hiatus periods. Nat Clim Chang 1(7):360–364

Minobe S, Kuwano-Yoshida A, Komori N, Xie SP, Small RJ (2008) Influence of the Gulf Stream on the troposphere. Nature 452(7184):206–209

Moore G, Renfrew I (2002) An assessment of the surface turbulent heat fluxes from the NCEP-NCAR reanalysis over the western boundary currents. J Clim 15(15):2020–2037

Qiu B, Chen S (2006) Decadal variability in the large-scale sea surface height field of the South Pacific Ocean: observations and causes. Journal of physical oceanography 36(9):1751–1762

Qiu B, Joyce TM (1992) Interannual variability in the mid-and low-latitude western North Pacific. J Phys Oceanogr 22(9):1062–1079

Ridgway K (2007) Long-term trend and decadal variability of the southward penetration of the East Australian Current. Geophys Res Lett 34(13)

Ridgway K, Coleman R, Bailey R, Sutton P (2008) Decadal variability of East Australian Current transport inferred from repeated high-density XBT transects, a CTD survey and satellite altimetry. J Geophys Res Oceans (1978–2012) 113(C8)

Roemmich D, Gilson J, Davis R, Sutton P, Wijffels S, Riser S (2007) Decadal spinup of the South Pacific subtropical gyre. J Phys Oceanogr 37(2):162–173

Sakamoto TT, Hasumi H, Ishii M, Emori S, Suzuki T, Nishimura T, Sumi A (2005) Responses of the Kuroshio and the Kuroshio Extension to global warming in a high-resolution climate model. Geophys Res Lett 32(14)

Santorelli A, Pinker R, Bentamy A, Katsaros K, Drennan W, Mestas-Nuñez A, Carton J (2011) Differences between two estimates of air-sea turbulent heat fluxes over the Atlantic Ocean. J Geophys Res Oceans (1978–2012) 116(C9)

Sato Y, Yukimoto S, Tsujino H, Ishizaki H, Noda A (2006) Response of North Pacific ocean circulation in a Kuroshio-resolving ocean model to an Arctic Oscillation (AO)-like change in northern hemisphere atmospheric circulation due to greenhouse-gas forcing. J Meteorol Soc Jpn 84(2):295–309

Shaman J, Samelson R, Skyllingstad E (2010) Air-sea fluxes over the Gulf Stream region: atmospheric controls and trends. J Clim 23(10):2651–2670

Tanimoto Y, Nakamura H, Kagimoto T, Yamane S (2003) An active role of extratropical sea surface temperature anomalies in determining anomalous turbulent heat flux. J. Geophys. Res 108(c10):3304. doi:10.1029/2002JC001750

Thompson DW, Wallace JM (2000) Annular modes in the extratropical circulation. Part I: month-to-month variability. J Clim 13(5):1000–1016

Tomita H, Kubota M (2005) Increase in turbulent heat flux during the 1990s over the Kuroshio/Oyashio extension region. Geophys Res Lett 32(9):L09,705

Uppala SM, Kållberg P, Simmons A, Andrae U, Bechtold V, Fiorino M, Gibson J, Haseler J, Hernandez A, Kelly G et al (2005) The ERA-40 re-analysis. Q J R Meteorol Soc 131(612):2961–3012

Woodruff SD, Worley SJ, Lubker SJ, Ji Z, Eric Freeman J, Berry DI, Brohan P, Kent EC, Reynolds RW, Smith SR et al (2011) ICOADS Release 2.5: extensions and enhancements to the surface marine meteorological archive. Int J Climatol 31(7):951–967

Wu L, Cai W, Zhang L, Nakamura H, Timmermann A, Joyce T, McPhaden MJ, Alexander M, Qiu B, Visbeck M et al (2012) Enhanced warming over the global subtropical western boundary currents. Nat Clim Chang 2(3):161–166

Yu L, Weller RA (2007) Objectively analyzed air–sea heat fluxes for the global ice-free oceans (1981–2005). Bull Am Meteorol Soc 88(4)

Yu L, Jin X, Weller RA (2008) Multidecade global flux datasets from the Objectively Analyzed Air-sea Fluxes (OAFlux) project: latent and sensible heat fluxes, ocean evaporation, and related surface meteorological variables. Tech. rep., OAFlux Project Tech. Rep. OA-2008-01

Zeng X, Zhao M, Dickinson RE (1998) Intercomparison of bulk aerodynamic algorithms for the computation of sea surface fluxes using TOGA COARE and TAO data. J Clim 11(10):2628–2644

Zhang GJ, Mcphaden MJ (1995) The relationship between sea surface temperature and latent heat flux in the equatorial Pacific. J Clim 8(3):589–605

Zhang L, Wu L, Lin X, Wu D (2010a) Modes and mechanisms of sea surface temperature low-frequency variations over the coastal China seas. J Geophys Res 115(C8):C08,031

Zhang W, Li J, Zhao X (2010b) Sea surface temperature cooling mode in the Pacific cold tongue. J Geophys Res Oceans (1978–2012) 115(C12)